

**A NEW DYNAMICAL PARAMETER FOR THE STUDY OF STICKY ORBITS IN A 3D GALACTIC MODEL**

Euaggelos E. Zotos

*Department of Physics, Section of Astrophysics, Astronomy and Mechanics,  
Aristotle University of Thessaloniki, 541 24, Thessaloniki, Greece;  
evzotos@astro.auth.gr*

Received: 2011 August 16; revised September 28; accepted: October 10

**Abstract.** A 3D dynamical model is used to study the motion in the central parts of an elliptical galaxy, hosting a massive and dense nucleus. Our aim is to investigate the regular or chaotic character of the motion, with emphasis in the different chaotic components, as well as the sticky regions of the dynamical system. In order to define the character of the motion in the 2D system, we use the classical method of the Poincaré  $x - p_x$  phase plane, the Lyapunov Characteristic Exponent (LCE) and the dynamical parameter – the  $S(c)$  spectrum. Then the results obtained from the 2D system are used to investigate the properties of the 3D system. For this, we introduce and use a new dynamical parameter, the  $S(k)$  spectrum, which proves to be a very reliable and fast method to detect the islandic motion and the evolution of the sticky orbits in the 3D system. Numerical experiments conducted by the new  $S(k)$  spectrum suggest that the different chaotic components in the 3D system do not interact for time intervals much larger than the age of the galaxy. The results indicate that the different sticky regions do not lead to a unified chaotic sea. Thus, the behavior of the 3D sticky orbits differs from that observed in the 2D system. Furthermore, the 3D motion near the center of a triaxial elliptical galaxy seems to be very complicated, displaying several families of resonant orbits, different chaotic components and sticky regions, while only a small fraction of orbits is regular. The comparison with earlier results reveals the importance of the conception of the new dynamical spectrum.

**Key words:** galaxies: kinematics and dynamics**1. INTRODUCTION**

Now it is evident that elliptical galaxies hosting massive and dense nuclei do exist (see Barth et al. 1999, 2001; Ho et al. 1995, 1997, 2000; Kaneda et al. 2005; Lauer et al. 2005; Maoz et al. 2005; Nagar et al. 2005; Shields et al. 2000). Therefore it is important to investigate the dynamical behavior of stars in the central parts of triaxial elliptical galaxies. For the study of a real elliptical galaxy with the particular overall density distribution, we choose a simple dynamical model based on the well-known logarithmic potential (see Binney & Tremaine 2008). We expand this potential in a Taylor series near the origin ( $x = 0$ ) with

the terms up to the second degree in the variables. This expansion is valid only within certain distances from the galaxy center. In our case, the calculation of orbits has been done up to the distances  $R = \sqrt{x^2 + y^2 + z^2} \leq 1$  from the center, hinting that only up to these distances the harmonic potential derived from the logarithmic expansion is valid (see the Appendix for more details about the Taylor expansion).

In the present study we investigate the motion of a test particle (star) in a 3D gravitational galactic potential consisting of two parts: the first part is the potential of a 3D anisotropic harmonic oscillator (for details see Kandrup & Sideris 2002 and Kandrup & Siopis 2003), derived from the Taylor expansion of the logarithmic potential, and the second part is a Plummer potential of a spherically symmetric nucleus. Our 3D dynamical model is

$$V(x, y, z) = \frac{\omega^2}{2} (x^2 + ay^2 + bz^2) - \frac{M_n}{\sqrt{x^2 + y^2 + z^2 + c_n^2}}. \quad (1)$$

The Plummer sphere which describes the potential of the spherical nucleus, has been applied several times in the past to study the effect of the introduction of a central mass component in a galaxy (see Hasan & Norman 1990; Hasan et al. 1993). Here  $a$  and  $b$  are parameters,  $M_n$  and  $c_n$  are the mass and the scale length of the nucleus, while the parameter  $\omega$  is used for the consistency of the galactic units. We use a system of galactic units, where the unit of mass is  $2.325 \times 10^7 M_\odot$ , the unit of length is 1 kpc and the unit of time is  $0.997748 \times 10^8$  yr. The velocity unit is 10 km/s, while  $G$  is equal to unity. In the above units we use the values:  $\omega = 10 \text{ km s}^{-1} \text{ kpc}^{-1}$ ,  $a = 4$ ,  $b = 1.25$ ,  $M_n = 50$ , while  $c_n$  is treated as a parameter. The test particle (star) which moves under the influence of the gravitational potential (1) is considered to have the mass  $m = 1$ .

There are two basic reasons justifying the choice of the potential (1). First, this simple potential can reasonably describe the character of orbits in the central parts of a triaxial elliptical galaxy. The second and most important reason is that the above potential displays important characteristics of the motion, such as a large variety of resonant orbits, different chaotic components and remarkable sticky regions. Therefore, it seems challenging to investigate the nature of the above characteristics, in order to draw some useful conclusions regarding the behavior of orbits in the central region of a triaxial elliptical galaxy, hosting a dense and massive nucleus.

The Hamiltonian to the potential (1) writes

$$H = \frac{1}{2} (p_x^2 + p_y^2 + p_z^2) + V(x, y, z) = h, \quad (2)$$

where  $p_x, p_y$  and  $p_z$  are the momenta per unit mass conjugate to  $x, y$  and  $z$  respectively, while  $h$  is the numerical value of the Hamiltonian. The outcomes of this research are based on the numerical integration of the equations of motion

$$\begin{aligned} \dot{x} &= p_x, & \dot{y} &= p_y, & \dot{z} &= p_z, \\ \dot{p}_x &= -\frac{\partial V(x, y, z)}{\partial x}, \\ \dot{p}_y &= -\frac{\partial V(x, y, z)}{\partial y}, \end{aligned}$$

$$\dot{p}_z = -\frac{\partial V(x, y, z)}{\partial z}, \quad (3)$$

where the dot indicates derivative with respect to the time. We use a Bulirsh – Stör integration routine in Fortran 95, with double precision in all subroutines. The accuracy of the outcomes was checked by constancy of the energy integral (2), which was conserved up to the fifteenth significant figure.

In order to distinguish between the regular or chaotic motion in different chaotic components, we use the Lyapunov Characteristic Exponent (LCE), see Lichtenberg & Lieberman (1992). Moreover, in order to be able to visualize and study the sticky and islandic motion in the 2D system, we use a dynamical parameter – the  $S(c)$  spectrum. Dynamical spectra have been frequently used over the last years for obtaining fast and reliable results regarding the regular or chaotic nature of orbits. Recently, new definitions of the dynamical spectra have been introduced in order to identify the regular or chaotic nature of orbits in the Hamiltonian systems of two (2D) and three (3D) degrees of freedom (see Zotos 2011a,b).

Here we must remind to the reader that this spectrum is the distribution function of the parameter  $c$

$$S(c) = \frac{\Delta N(c)}{N\Delta c}, \quad (4)$$

where  $\Delta N(c)$  is the number of the parameters  $c$  in the interval  $(c, c + \Delta c)$  after  $N$  iterations. The parameter  $c$  is defined as

$$c_i = \frac{x_i - p_{xi}}{p_{yi}}, \quad (5)$$

where  $(x_i, p_{xi}, p_{yi})$  are the successive values of the  $(x, p_x, p_y)$  elements of a 2D orbit on the Poincaré  $x - p_x, y = 0, p_y > 0$  phase plane. More details regarding the shapes and behavior of dynamical spectra can be found in Caranicolas & Papadopoulos (2007) and Caranicolas & Zotos (2010).

The layout of this article is as follows: in Section 2 we study the behavior of orbits in the 2D system. In the same Section a systematic presentation of sticky regions is made, and the evolution of sticky orbits is investigated using the  $S(c)$  spectrum. Furthermore, we study the degree of chaos in the different chaotic components of the model applying the values of LCE. We try to find out the role of the scale length  $c_n$  of the nucleus in the evolution of different chaotic components. In Section 3 we investigate a 3D model, using a new dynamical indicator, the  $S(k)$  spectrum. Here we are interested to find out if the different chaotic components in the 2D system merge in order to form a 3D unified chaotic manifold. Another interesting question is to determine the initial conditions in the  $H(x, p_x, z) = h, p_y > 0, (y = p_z = 0)$  phase space, giving rise to regular or chaotic orbits. Finally, in Section 4 we present a discussion and the conclusions of this research.

## 2. THE STRUCTURE OF THE 2D DYNAMICAL SYSTEM

Let us now proceed to study the character of orbits in a 2D model. The corresponding 2D Hamiltonian is

$$H_2 = \frac{1}{2}(p_x^2 + p_y^2) + V(x, y) = h_2, \quad (6)$$

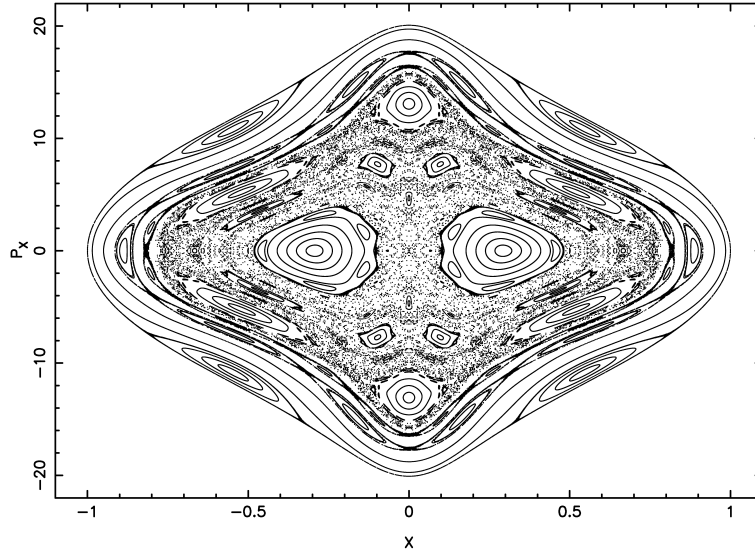


**Fig. 1.** The  $x - p_x$  phase plane, when  $h_2 = 1.5$ . Details are given in the text.

where  $h_2$  is the numerical value of Hamiltonian (6). Figure 1 shows the  $x - p_x$  phase plane for this Hamiltonian when  $h_2 = 1.5$ . The values of the parameters are:  $\omega = 10$ ,  $a = 4$ ,  $b = 1.25$ ,  $M_n = 50$  and  $c_n = 0.25$ . As one can see, this is a very interesting and complicated phase plane, with considerable sticky regions, sets of islands of invariant curves produced by a number of secondary resonances and several different chaotic components. In order to help the reader, we will describe in detail each of the above cases.

Figures 2(a)–(d) show the three sticky regions observed in the  $x - p_x$  phase plane of the dynamical system. Figure 2a shows the sticky region I, consisting of two large sticky islands. The initial conditions are:  $x_0 = \pm 0.1$ ,  $p_{x0} = 0$  and the integration time is 2000 time units. Figure 2b shows the sticky region II consisting of eight islands. The initial conditions are:  $x_0 = 0.06$ ,  $p_{x0} = 6.77$  and the integration time is 900 time units. Note that the four sticky islands are produced by one sticky orbit, while the other four are produced by the twin symmetric sticky orbit traversed in the opposite direction. Figure 2c shows the sticky region III composed of six sticky islands produced by the two twin orbits. The initial conditions are:  $x_0 = 0$ ,  $p_{x0} = 10.5$  and the integration time is 750 time units. Each sticky orbit produces three sticky islands. Figure 2d shows all three sticky regions which are embedded in the chaotic sea. This chaotic sea is the place, where the test particle (star) ends after each sticky period. The integration time of each region shown in Figures 2(a–d) is equal to each sticky period.

The evolution of sticky orbits can be followed using the  $S(c)$  spectrum. The results are shown in Figures 3(a)–(d). Figure 3a shows the spectrum of an orbit producing three islands. The initial conditions are:  $x_0 = 0$ ,  $y_0 = 0$ ,  $p_{x0} = 12.6$ , while the value of  $p_{y0}$  is always found from the energy integral (6). The values of all other parameters are as in Figure 1. Here we observe three well defined  $U$ -type spectra, indicating a regular motion. Note that the number of spectra is equal to the number of islands. Figure 3b shows the  $S(c)$  spectrum of an orbit starting near

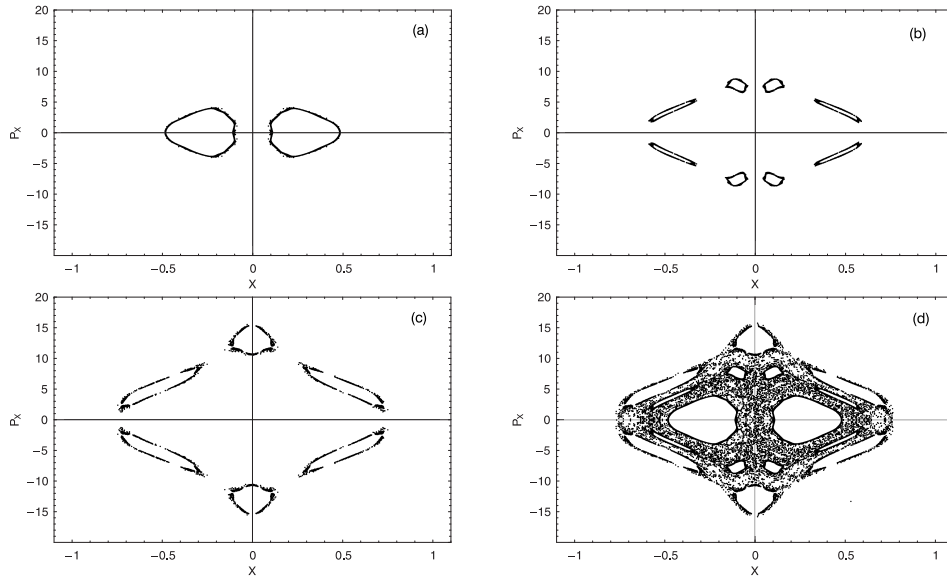


**Fig. 2.** Panels (a)–(c): the three sticky regions and panel (d): the sticky regions embedded in the chaotic sea.

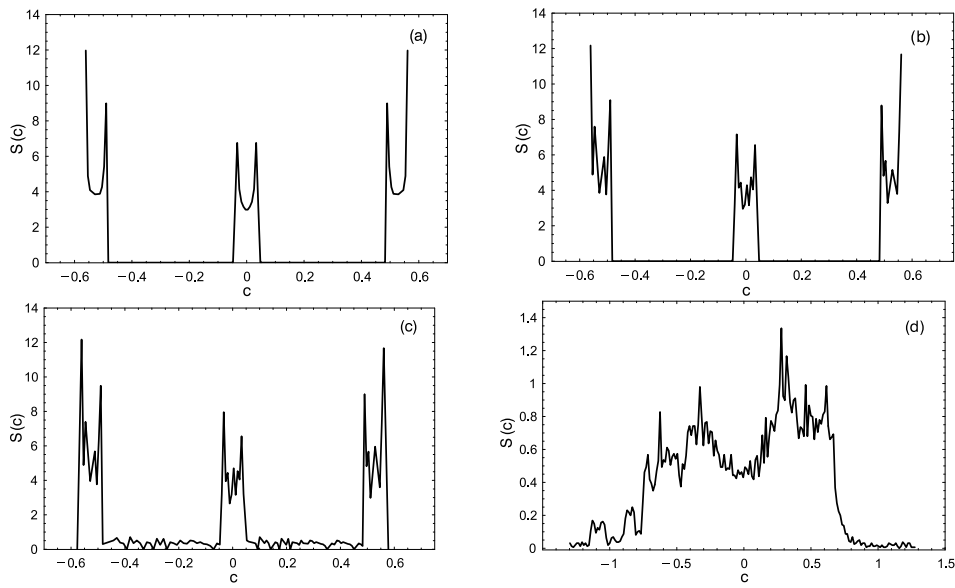


**Fig. 3.** Panel (a): the  $S(c)$  spectrum of a nearby quasi-periodic orbit and panels (b)–(d): evolution of the  $S(c)$  spectrum for a sticky orbit.

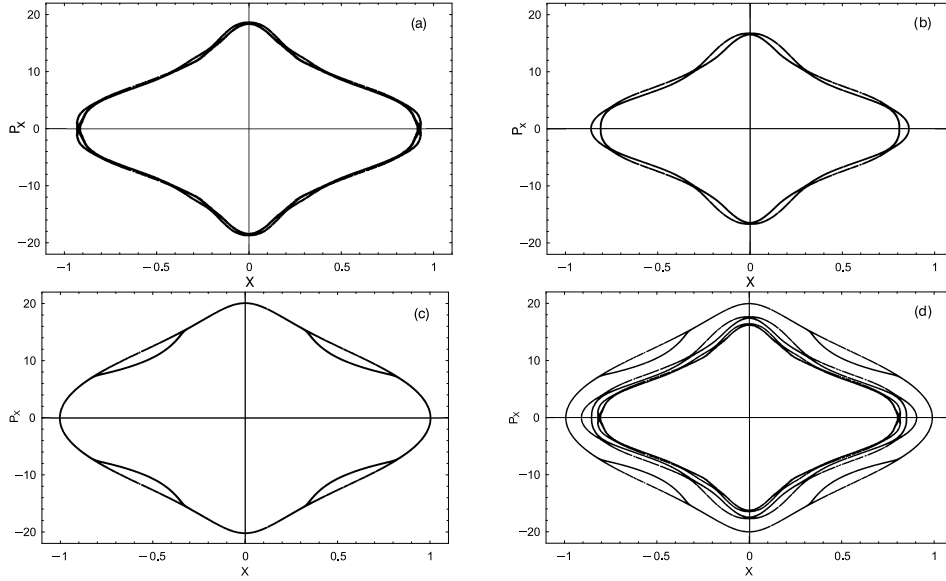


**Fig. 4.** Panels (a)–(c): the three chaotic components and panel (d): all the chaotic components together.

the above regular orbit. The initial conditions are:  $x_0 = 0$ ,  $y_0 = 0$ ,  $p_{x0} = 10.5$ . Here we observe three different spectra with a number of large and small peaks. This indicates that we have a sticky orbit, and the sticky region is composed of the three sticky islands. The sticky period is about  $T = 720$  time units. Figure 3c shows the spectrum of the same orbit when  $T = 780$ . Here, the three spectra have merged to produce a unified spectrum. This indicates that after the sticky period the test particle (star) has moved to the chaotic sea. Figure 3d shows the spectrum of the orbit when  $T = 3000$ . Here we observe the spectrum of a chaotic orbit with a large number of small and large asymmetric peaks. Note that the sticky period obtained from the  $S(c)$  spectrum is very close to the integration time of Figure 2c. The  $S(c)$  spectrum shows that in all sticky regions of the dynamical system the sticky period is between 700–900 time units and finally the test particle (star) ends in the chaotic sea surrounding all the three sticky regions.

Figures 4(a)–(d) show the different chaotic components observed in the  $x - p_x$  phase plane of the dynamical system. Figure 4a shows the chaotic component I with the initial conditions  $x_0 = -0.82$  and  $p_{x0} = 0$ . Figure 4b shows the chaotic component II with the initial conditions  $x_0 = -0.86$  and  $p_{x0} = 0$ . Figure 4c shows the chaotic component III with the initial conditions  $x_0 = -1$  and  $p_{x0} = 0$ . All the three chaotic components together are shown in Figure 4d. The above three chaotic components, together with the chaotic sea shown in Figure 2d, are the four chaotic components of the 2D system. The integration time of the chaotic components, shown in Figures 4(a)–(d), is 2000 time units. As expected, each chaotic component has its own value of LCE (see Saito & Ichimura 1979). A plot of LCEs for a time period of  $10^5$  time units is shown in Figure 5. I, II, III indicate the three chaotic components, while S stands for the chaotic sea. The LCE for the chaotic component I has the value 0.8372, for the chaotic component II the value

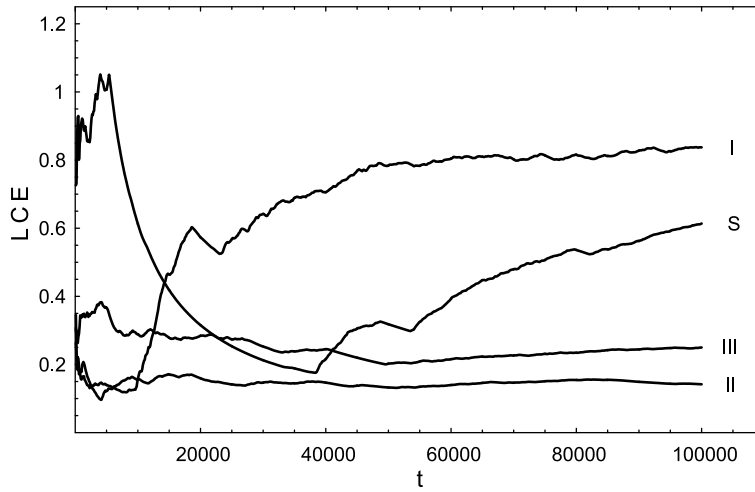


**Fig. 5.** The LCEs for the three different chaotic components I, II, III and the chaotic sea S.

0.1423 and for the chaotic component III the value 0.2512. The LCE value for the chaotic sea is 0.6137.

Figures 6 (a)–(h) show eight typical periodic orbits for the 2D dynamical system. The values of all other parameters are as in Figure 1. Figure 6a shows a periodic orbit characteristic to the 1:1 resonance, while the orbits shown in Figures 6b, 6c, 6d, 6e, 6f, 6g and 6h are periodic orbits characteristic to the 1:2, 2:3, 3:4, 3:5, 4:5, 5:7 and 5:8 resonant families, respectively. In all 2D orbits  $y_0 = 0$ , while the value of  $p_{y0}$  is always found from the energy integral (6). The values of the initial conditions are given in the caption. The integration time for all orbits, shown in Figures 6 (a)–(h), is 100 time units. It is remarkable that all the above resonances are present in the simple 2D Hamiltonian (6). The interaction of all these resonances justifies the presence of the different sticky regions and also the four different chaotic components.

Figure 7 is similar to Figure 1 but corresponds to  $c_n = 0.1$  and  $h_2 = 0.25$ . The only physical difference here is that we have a more dense nucleus. In this case, all the above chaotic components have merged to produce one chaotic ocean. There are only two sets of islands. The set of the invariant curves in the two large islands on the  $x$ -axis is produced by quasi-periodic orbits typical for the 1:1 resonance, while the set of the four islands is produced by quasi-periodic orbits typical for the 1:2 resonance. Note that these resonances are the basic ones of the system, since the 1:1 resonance originates from the potential of the nucleus, and the 1:2 resonance originates from the potential of the anisotropic harmonic oscillator. There is only one sticky region left at the boundary between the set of the large islands and the chaotic ocean. Another interesting property is the increase in the velocity near the central region of Figure 7. Therefore, one can conclude that the nuclei with moderate densities produce considerable sticky motions, different chaotic regions and a large number of resonances. On the other hand, the nuclei with high densities produce large unified chaotic regions. The degree of chaos in this case is high, as the value of the LCE for a set of different initial conditions

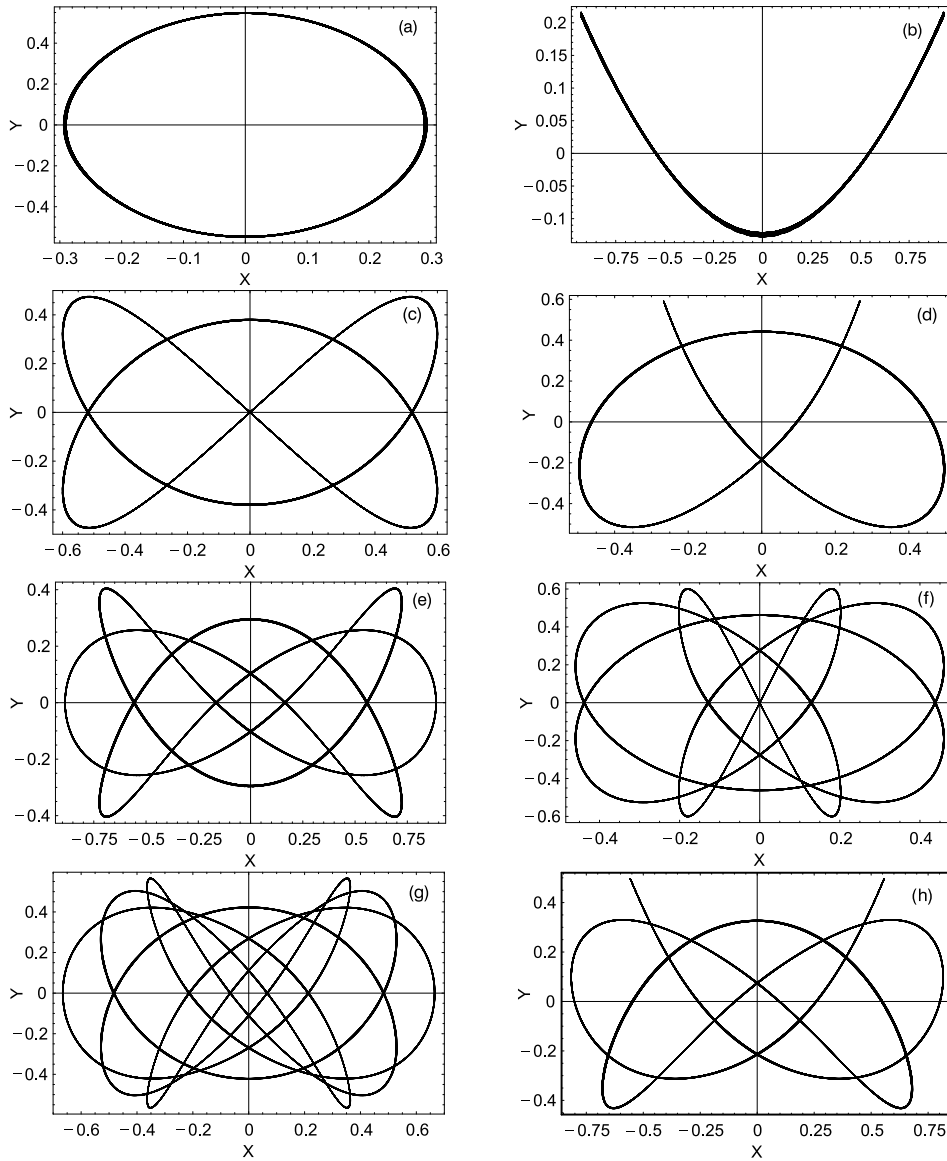


**Fig. 6.** Panels (a)–(h): representative periodic orbits in the 2D dynamical system. The initial conditions are (a):  $x_0 = 0.2943$ ,  $p_{x0} = 0$ ; (b):  $x_0 = 0.548$ ,  $p_{x0} = 10.8$ ; (c):  $x_0 = 0$ ,  $p_{x0} = 13.07$ ; (d):  $x_0 = 0.097$ ,  $p_{x0} = 7.7$ ; (e):  $x_0 = 0.889$ ,  $p_{x0} = 0$ ; (f):  $x_0 = 0$ ,  $p_{x0} = 4.675$ ; (g):  $x_0 = 0.667$ ,  $p_{x0} = 0$  and (h):  $x_0 = 0.803$ ,  $p_{x0} = 2.03$ .

on the chaotic ocean and a time period of  $10^5$  time units was found to tend to the value 4.25. Furthermore, it is evident that this chaotic motion happens at high velocities.



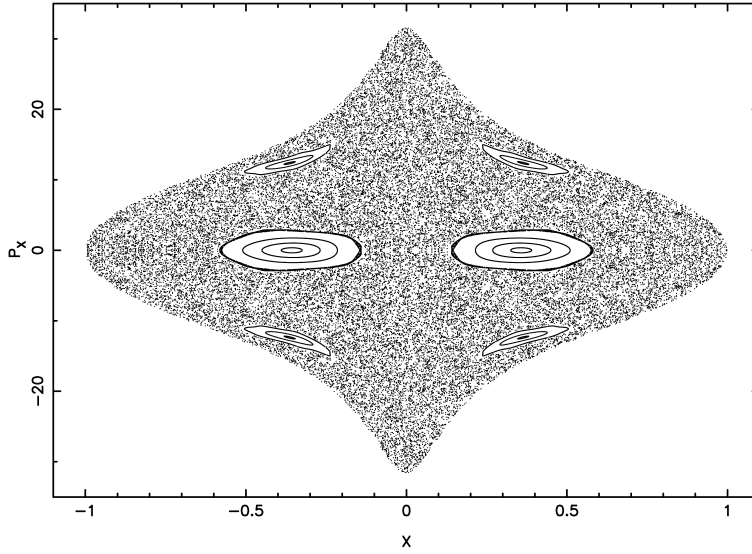


**Fig. 7.** Similar to Figure 1, but for  $c_n = 0.10$  and  $h_2 = 0.25$ .

### 3. THE STRUCTURE OF THE 3D DYNAMICAL SYSTEM

In this Section, the results regarding the character of motion in the 3D system will be presented. For this purpose we use the 3D Hamiltonian (2) and take  $h = h_2$ , i.e., the value of energy is equal to that in the 2D system. The results obtained in the 2D system will be used to investigate the motion in the 3D system. We consider orbits with a starting point on the  $x - p_x$  phase plane with an additional value of  $z = z_0$  and follow the evolution of 3D orbits.

As a first step in this investigation, we decided to compute the LCEs for orbits with the initial conditions  $(x_0, p_{x0}, z_0)$ , where  $(x_0, p_{x0})$  is a point in each of the chaotic components of the 2D system (see Figures 1 and 4). The values of  $y_0$  and  $p_{z0}$  are always taken equal to zero, while the value of  $p_{y0}$  is always found from the energy integral (2). Figure 8 is similar to Figure 5 but corresponds to the 3D system. It is interesting to observe, that each chaotic component has again a different value of LCE. The LCE values were found to be 0.4231, 0.0007 and 0.1923 in the chaotic components I, II and III respectively. In the chaotic sea the LCE has the value 0.4562. Note that all the LCE values for the 3D system are smaller than the corresponding values of the 2D system. For the computation of the LCE values of the chaotic components we used the value  $z_0 = 0.1$ .

This strongly indicates, that the different chaotic components of the 3D system do not merge to produce a single unified chaotic region. This result is compatible with the outcomes of Cincotta et al. (2006), where no evidence is found that in 3D systems with a divided phase space a completely unified chaotic manifold actually exists. On the other hand, in the case of the dense nucleus, where we have only one chaotic component, all tested 3D orbits with the initial conditions  $(x_0, p_{x0}, z_0)$  (where  $(x_0, p_{x0})$  is a point at the chaotic ocean) lead to a common value of LCE close to 1.65.

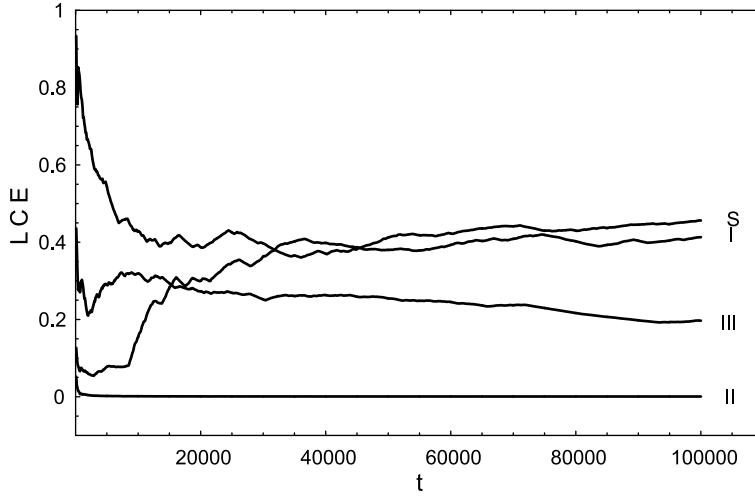


**Fig. 8.** Similar to Figure 5, but for the 3D model.

Our next step is to see what happens to orbits with the initial conditions  $(x_0, p_{x0}, z_0)$ , where  $(x_0, p_{x0})$  is a point in the regular or chaotic regions of the phase plane of Figure 1. For this purpose we introduce and use a new type of dynamical parameter – the  $S(k)$  spectrum. The parameter  $k_i$  is defined as

$$k_i = \frac{(x_i + z_i) - (p_{xi} + p_{zi})}{p_{yi}}, \quad (7)$$

where  $(x_i, z_i, p_{xi}, p_{yi}, p_{zi})$  are the successive values of  $(x, z, p_x, p_y, p_z)$  elements of the 3D orbit. We will call as the dynamical spectrum of the parameter  $k$  its distribution function

$$S(k) = \frac{\Delta N(k)}{N \Delta k}, \quad (8)$$

where  $\Delta N(k)$  is the number of the parameters  $k$  in the interval  $(k, k + \Delta k)$  after  $N$  iterations. By definition, the  $k$  parameter is based on a complicated combination of coordinates and velocities of the 3D orbit. There are several reasons for introducing the  $S(k)$  spectrum: (1) it can identify 3D islandic motion, (2) it can help us to understand the evolution of 3D sticky orbits, and (3) it is much faster than other dynamical indicators, such as the LCE, SALI (Smaller ALignment Index, see Skokos 2001) or and GALI (Generalized ALignment Index, see Skokos et al. 2007), which need time periods of the order of  $10^5$  time units to give reliable results.

Figure 9a shows the  $S(k)$  spectrum for a 3D regular orbit, with the initial conditions:  $x_0 = 0.24$ ,  $p_{x0} = p_{z0} = 0$ ,  $z_0 = 0.001$ , while the value of  $p_{y0}$  is found from the energy integral (2). As expected, a well defined U-type spectrum is observed, indicating a regular motion. The corresponding LCE for a regular 3D orbit and a time period of  $10^5$  time units is given in Figure 9b. Figure 9c shows the  $S(k)$  spectrum for a 3D chaotic orbit, with the initial conditions:  $x_0 = 0.76$ ,  $p_{x0} = 1.4$ ,  $p_{z0} = 0$ ,  $z_0 = 0.3$ , and the value of  $p_{y0}$  is found from the energy integral (2). Here, we can see a complicated and asymmetric spectrum, with a lot

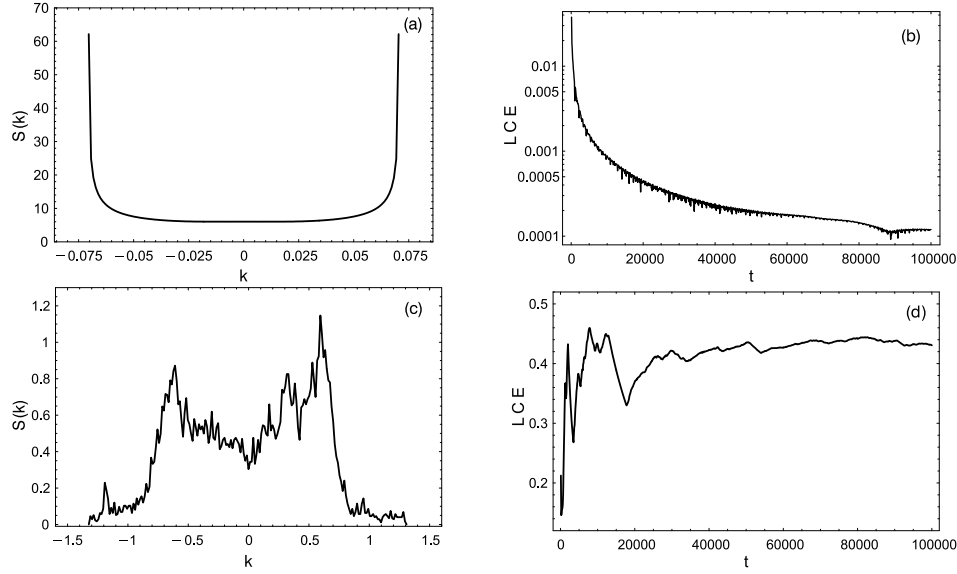


**Fig. 9.** Panel (a): the  $S(k)$  spectrum for a 3D regular orbit, panel (b): the corresponding LCE of a 3D regular orbit, panel (c): the  $S(k)$  spectrum for a 3D chaotic orbit and panel (d): the corresponding LCE of a 3D chaotic orbit.

of large and small peaks. This is a typical  $S(k)$  spectrum of a chaotic orbit. The corresponding LCE for a 3D chaotic orbit and a time period of  $10^5$  time units is given in Figure 9d. The integration time for both spectra shown in Figures 9a and 9c is 3000 time units.

Let us now start with the orbits with the initial conditions  $(x_0, p_{x0})$  in the islands of Figure 2a. Using the  $S(k)$  spectrum it was found that for all  $(x_0, p_{x0})$  in the regions of Figure 2a, when  $z_0 \leq 0.0065$ , the motion is regular, while for all larger permitted values of  $z_0$  the motion becomes chaotic.

Interesting results are obtained for the initial conditions  $(x_0, p_{x0}, z_0)$ , where  $(x_0, p_{x0})$  is a point in the regular region inside one of the four islands in the phase plane of Figure 2b. Remember that in Figure 2b we see eight islands produced by the two identical orbits traversed in opposite directions. Each of these orbits produces four islands. Figure 10(a)–(d) shows the  $S(k)$  spectrum of two such orbits. Figure 10a shows the  $S(k)$  spectrum for an orbit producing the set of four islands shown in Figure 2b. The initial conditions are:  $x_0 = 0.09$ ,  $p_{x0} = 7.5$ ,  $z_0 = 0.01$ ,  $y_0 = p_{z0} = 0$ . As expected, we observe four well defined U-type spectra. The motion is regular. Figure 10b shows the  $S(k)$  spectrum for the orbit starting near the above described regular orbit. The initial conditions are:  $x_0 = 0.09$ ,  $p_{x0} = 7.5$ ,  $z_0 = 0.05$ ,  $y_0 = p_{z0} = 0$ . Here we see again the four spectra, each one corresponding to an island. Figure 10b exhibits some additional small peaks which indicate a 3D sticky motion.

Let us now look at the evolution of a 3D sticky orbit using the  $S(k)$  spectrum. The sticky period is about 1200 time units. Figure 10c shows the  $S(k)$  spectrum of a sticky orbit, about 100 time units after the test particle (star) has left the sticky region. Here, the four spectra have been joined together producing a single

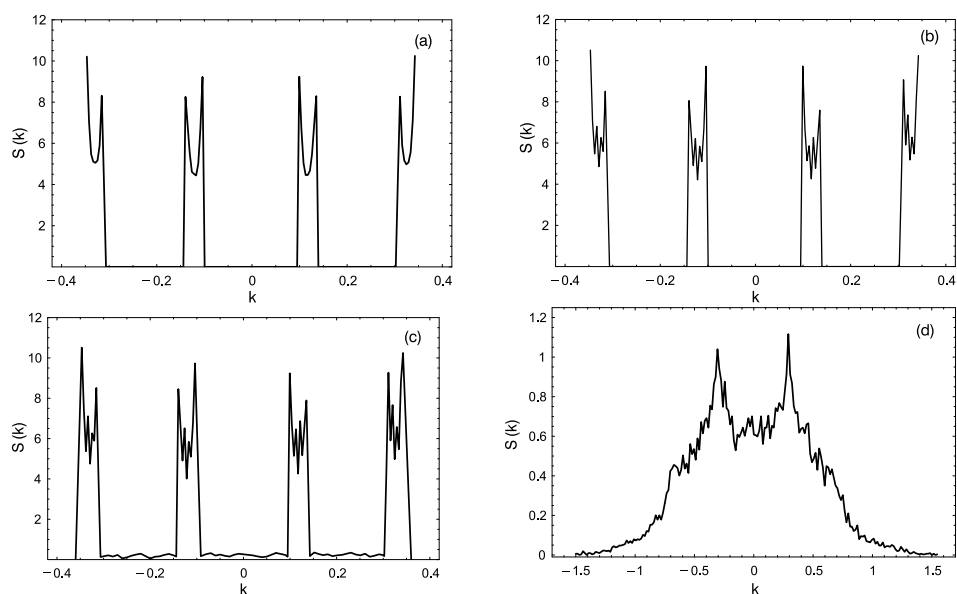


**Fig. 10.** Panel (a): the  $S(k)$  spectrum of a 3:4 resonant 3D orbit. Panels (b)–(d): the evolution of the  $S(k)$  spectrum of a sticky 3D orbit. See the text for details.

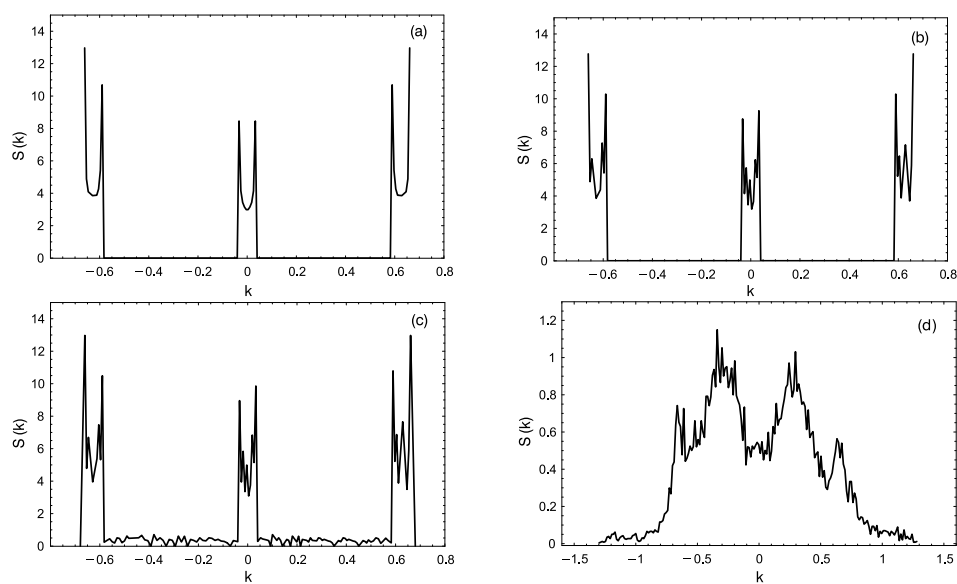


**Fig. 11.** Panel (a): the  $S(k)$  spectrum of a 2:3 resonant 3D orbit. Panels (b)–(d): the evolution of the  $S(k)$  spectrum of a sticky 3D orbit. See the text for details.

spectrum. This spectrum has the characteristics of a chaotic spectrum and this strongly suggests that the test particle (star) has left the sticky region and entered to the chaotic component. The shape of the  $S(k)$  spectrum, after the test particle (star) has traveled 5000 time units in the chaotic component, is shown in Figure 10d. Our numerical experiments give similar results for other initial conditions  $(x_0, p_{x0}, z_0)$ , where  $(x_0, p_{x0})$  is a point inside one of the four islands of invariant curves shown in Figure 2b. Therefore, we come to the conclusion that the orbits which start inside the set of the four islands, produced by the 3:4 resonance and having  $z_0 \leq 0.038$ , are regular while for larger values of  $z_0$  the orbits become sticky, with a sticky period of about 1200 time units.

Things are similar for the orbits with the initial conditions  $(x_0, p_{x0}, z_0)$ , where  $(x_0, p_{x0})$  is a point in the regular region inside one of the three islands in the phase plane of Figure 2c. Remember again that in Figure 2c we observe six islands produced by two identical orbits traversed in opposite directions. Each of these orbits produces three islands. Figure 11a shows the  $S(k)$  spectrum of an orbit with the initial conditions:  $x_0 = 0$ ,  $p_{x0} = 12.8$ ,  $z_0 = 0.01$ ,  $y_0 = p_{z0} = 0$ , and the value of  $p_{y0}$  found from the energy integral (2). The values of all other parameters are as in Figure 1. Here we observe three well defined  $U$ -type spectra indicating a regular motion. Note that the number of spectra is equal to the number of islands. Figure 11b shows the  $S(k)$  spectrum of an orbit starting near the above regular orbit. The initial conditions are:  $x_0 = 0$ ,  $p_{x0} = 12.8$ ,  $z_0 = 0.05$ ,  $y_0 = p_{z0} = 0$ . Here we observe three different spectra with a number of large and small peaks. This indicates that we have a 3D sticky orbit, and the sticky region is composed of three sticky islands. The sticky period is about  $T = 1700$  time units. Figure 11c shows the spectrum of the same orbit when  $T = 1800$ . Here the three spectra have merged to produce a unified spectrum. This indicates that after the sticky period, the test particle (star) has gone to the 3D chaotic component. In Figure 11d we see the spectrum of the orbit when  $T = 7000$ . Here the spectrum of a chaotic orbit shows a large number of small and large asymmetric peaks. Our numerical experiments give similar results for different initial conditions,  $(x_0, p_{x0}, z_0)$ , where  $(x_0, p_{x0})$  is a point inside one of the three islands of invariant curves shown in Figure 2c. Therefore, once more we conclude that the orbits which start inside the set of the three islands, produced by the 2:3 resonance and with  $z_0 \leq 0.042$ , are regular, while for larger values of  $z_0$  the orbits become sticky, with a sticky period of about 1700 time units. For each case of the resonant orbits we have computed about 100 orbits with different initial conditions in order to estimate the mean value for each sticky period.

Figures 12(a)–(h) show eight typical periodic orbits in the 3D dynamical system. In all orbits the values of the initial conditions  $(x_0, p_{x0})$  are the same as the 2D orbits, shown in Figures 6(a)–(h). For all 3D orbits  $y_0 = 0$ , the value of  $p_{y0}$  is found from the energy integral (2) and the value of  $z_0$  is 0.01. Note that all 3D periodic orbits shown in Figure 12(a)–(h) stay very close to the galactic plane. The integration time for all 3D periodic orbits, shown in Figures 12(a)–(h), is 100 time units.

#### 4. DISCUSSION AND CONCLUSIONS

In the present article we studied the orbital behavior in the central parts of a triaxial elliptical galaxy hosting a dense and massive nucleus. The main conclusions of our investigation are the following.

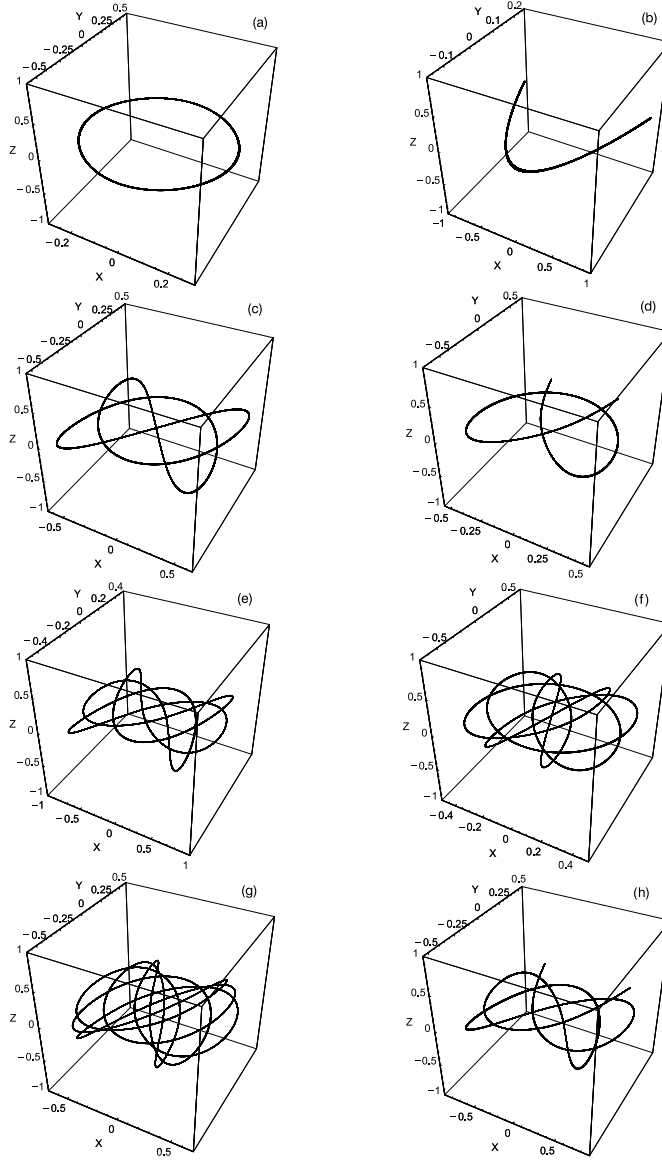


**Fig. 12.** Panels (a)–(h): representative periodic orbits in the 3D dynamical system. See the text for details.

1. The orbital analysis of the Hamiltonian system of the two degrees of freedom (2D) revealed a large variety of resonant orbits, different chaotic components and several sticky regions. The different chaotic components of the 2D system do not merge to produce a unified chaotic region, even for time intervals much larger than the age of the galaxy.

2. The results of the Hamiltonian system of the three degrees of freedom (3D)

are also of particular interest. Once more, the four different chaotic components of the 3D dynamical system continue to exist separately for vast time intervals, leading to the conclusion that the chaotic phase space of the 3D system remains divided.

The general conclusion – our model indicates that in the central region of triaxial elliptical galaxies the 3D motion is complicated, displaying several families of resonant orbits, different chaotic components and remarkable sticky regions, while only a small fraction of orbits is regular. This interesting galactic dynamical system can be used for testing the efficiency and reliability of other dynamical spectra introduced in previous papers (see Zotos 2011a,b). In particular, we can check if these new definitions can identify resonant orbits of higher multiplicity, different chaotic components and sticky regions both in 2D and 3D systems.

The  $S(k)$  spectrum is a very effective tool for the study of 3D motion, as it produces as much spectra as is the number of islands of invariant curves or, consequently, the number of the 3D invariant manifolds. Another advantage of the new spectrum is that it can be used for the calculation of the 3D sticky motion period. The  $S(c)$  spectrum can be also used to study the character of a 3D orbit, but it has no ability to detect the 3D sticky motion. The main reason is that the coupling of the third component,  $z$ , carrying all the information about 3D motion in general, is hidden in the definition of the  $S(c)$  spectrum, but in any case it affects the values of  $x$ ,  $p_x$  and  $p_y$  entering relation (5). Using the definition of the  $S(k)$  spectrum, we have managed to overtake this minor drawback, and we have constructed a new dynamical spectrum suitable for 3D orbits and especially for 3D sticky orbits. We must also point out, that when we deal with 2D motion, i.e. when ( $z = p_z = 0$ ), the  $S(k)$  spectrum transforms to  $S(c)$ .

**ACKNOWLEDGMENTS.** I am much indebted to Professor N. D. Caranicolas for drawing my attention to the study of 3D sticky orbits and for fruitful discussions during this research. I also thank Peeter Tenjes for careful reading the manuscript and for important suggestions and comments, which improved the quality of the present paper.

## APPENDIX. The Taylor expansion

In order to describe the motion in a triaxial elliptical galaxy, we use the well known logarithmic potential

$$V_L = \frac{v_0^2}{2} \ln [x^2 + ay^2 + bz^2 + c^2] , \quad (9)$$

where  $v_0$  is used for the consistency of the galactic units,  $a$  and  $b$  are flattening parameters and  $c$  is the scale parameter of the elliptical galaxy (see Caranicolas & Zotos 2011). Expanding potential  $V_L$  in Taylor series about the origin and keeping terms up to the second degree in the variables we find

$$\begin{aligned} V_T &= \frac{v_0^2}{2} \ln \left[ \left( \frac{x^2 + ay^2 + bz^2}{c^2} + 1 \right) c^2 \right] = \frac{v_0^2}{2} \ln c^2 + \frac{v_0^2}{2c^2} (x^2 + ay^2 + bz^2) \\ &= v_0^2 \ln c + \frac{v_0^2}{2c^2} (x^2 + ay^2 + bz^2) . \end{aligned} \quad (10)$$

Thus, the harmonic potential  $V_T$  which is derived from the logarithmic expansion is

$$V_T = \frac{\omega^2}{2} (x^2 + ay^2 + bz^2) , \quad (11)$$

where it was assumed that

$$\frac{x^2 + ay^2 + bz^2}{c^2} \ll 1 , \quad (12)$$

and

$$\omega = \frac{v_0}{2} . \quad (13)$$

We use the values:  $v_0 = 20$ ,  $a = 4$ ,  $b = 1.25$ ,  $c = 2$ . Here we must point out that these values of the involved parameters are valid only for distances  $R = \sqrt{x^2 + y^2 + z^2} \leq 1$  from the galactic center. We choose these particular values in order to describe and study only the central parts of the galaxy, where the sticky regions and the resonant phenomena take place. From the experience of our previous work we believe that typical values of the scale parameter,  $c$ , for an elliptical galaxy are in the range  $0.5 \leq c \leq 2.5$ .

#### REFERENCES

- Barth A. J., Filippenko A. V., Moran E. C. 1999, ApJ, 525, 673  
 Barth A. J., Ho L. C., Filippenko A. V. et al. 2001, ApJ, 546, 205  
 Binney J., Tremaine S. 2008, *Galactic Dynamics*, Princeton Series in Astrophysics, 2nd ed.  
 Caranicas N. D., Papadopoulos N. I. 2007, AN, 328, 556  
 Caranicas N. D., Zotos E. E. 2010, New Astronomy, 15, 427  
 Caranicas N. D., Zotos E. E. 2011, Research in Astronomy and Astrophysics, 11(7), 811  
 Cincotta P. M., Giordano C. M., Perez M. J. 2006, A&A, 455, 499  
 Hasan H., Norman C. A. 1990, ApJ, 361, 69.  
 Hasan H., Pfenniger D., Norman C. 1993, ApJ, 409, 91  
 Ho L. C., Filippenko A. V., Sargent W. L. W. 1995, ApJS, 98, 477  
 Ho L. C., Filippenko A. V., Sargent W. L. W. 1997, ApJS, 112, 315  
 Ho L. C., Rudnick G., Rix H. W. et al. 2000, ApJ, 541, 120  
 Kandrup H. E., Sideris I. V. 2002, CeMDA, 82, 61  
 Kandrup H. E., Siopis Ch. 2003, MNRAS, 345, 727  
 Kaneda H., Onaka T., Sakon I. 2005, ApJ, 632, L83  
 Lauer T. R., Faber S. M., Gebhardt K. et al. 2005, AJ, 129, 2138  
 Lichtenberg A. J., Lieberman M. A. 1992, *Regular and Chaotic Dynamics*, Springer, 2nd ed.  
 Maoz D., Nagar N. M., Falcke H., Wilson A. S. 2005, ApJ, 625, 699  
 Nagar N. M., Falcke H., Wilson A. S. 2005, A&A, 435, 521  
 Saito N., Ichimura A. 1979, in *Stochastic Behavior in Classical and Quantum Hamiltonian Systems*, eds. G. Casati & L. Ford, Springer, p.137  
 Shields J. C., Rix H. W., McIntosh D. H. et al. 2000, ApJ, 534, L27  
 Skokos Ch. 2001, J. Phys. A, 34, 10029  
 Skokos Ch., Bountis T. C., Antonopoulos Ch. 2007, Physica D, 231, 30



Zotos E. E. 2011a, *New Astronomy*, 16, 391

Zotos E. E. 2011b, *Baltic Astronomy*, 20, 75